Dorsal root ganglion stimulation for chronic pain modulates Aβ-fiber activity but not C-fiber activity: a computational modeling study

Robert D. Graham[a,b], Tim M. Bruns[a,b], Bo Duan[c], and Scott F. Lempka[a,b,d]

[a]Department of Biomedical Engineering, University of Michigan, Ann Arbor, MI, USA
[b]Biointerfaces Institute, University of Michigan, Ann Arbor, MI, USA
[c]Department of Molecular, Cellular, and Developmental Biology, University of Michigan, Ann Arbor, MI, USA
[d]Department of Anesthesiology, University of Michigan, Ann Arbor, MI, USA

Corresponding Author:
Scott F. Lempka, PhD
Department of Biomedical Engineering
University of Michigan
2800 Plymouth Road, NCRC 014-184
Ann Arbor, MI 48109-2800
Email: lempka@umich.edu

Abstract

Objective*:*

The goal of this project was to use computational models to investigate which types of primary sensory neurons are modulated by dorsal root ganglion stimulation (DRGS) to provide pain relief.

Methods:

We modeled DRGS by coupling an anatomical finite element model of a human L5 dorsal root ganglion to biophysical models of primary sensory neurons. We calculated the stimulation amplitude needed to elicit an action potential in each neuron, and examined how DRGS affected sensory neuron activity.

Results:

We showed that within clinical ranges of stimulation parameters, DRGS drives the activity of large myelinated Aβ-fibers but does not directly activate small nonmyelinated C-fibers. We also showed that the position of the active and return electrodes and the polarity of the stimulus pulse influence neural activation.

Conclusions:

Our results indicate that DRGS may provide pain relief by activating pain-gating mechanisms in the dorsal horn via repeated activation of large myelinated afferents.

Significance:

Understanding the mechanisms of action of DRGS-induced pain relief may lead to innovations in stimulation technologies that improve patient outcomes.

<u>Highlights</u>

- When using standard clinical parameters, DRGS does not activate C-fibers.
- Straddling the active and return electrodes across the DRG increases neural activation.
- DRGS may provide pain relief by activating pain-gating mechanisms in the spinal cord.

Keywords:

Chronic pain

Dorsal root ganglion

Computer simulation

Electric stimulation

Spinal cord stimulation

Acknowledgements

Technical assistance: The authors would like to thank Dr. Stephen McMahon (King's College London, London, UK) for his helpful comments and feedback on the multi-compartment neuron models.

Funding: This research was supported in part through computational resources provided by Advanced Research Computing at the University of Michigan, Ann Arbor, by the National Institutes of Health (NIH R01 NS089530), and by the National Science Foundation (NSF CAREER award 1653080).

Conflict of interest statement: SFL is a shareholder and scientific advisory board member of Presidio Medical, Inc. All other authors declare no conflicts of interest.

1. Introduction

Chronic pain is a debilitating disorder that affects over 100 million Americans and accounts for $560-635 billion in healthcare and productivity costs in the United States each year (Gaskin and Richard 2012). For patients with chronic pain that is refractory to conventional medical management (e.g. pharmaceuticals, orthopedic surgery), neurostimulation therapies, such as spinal cord stimulation (SCS) and dorsal root ganglion stimulation (DRGS), are alternative treatment options. SCS has been a mainstay of refractory pain management for decades, and is achieved by implanting electrode arrays in the epidural space dorsal to the spinal cord (Lempka and Patil 2018). The goal of conventional SCS is to apply electrical impulses to the region of the spinal cord that innervates the patient's painful region, which evokes paresthetic (i.e. tingling) sensations in that region to mask pain perception. Unfortunately, the anatomy of the spinal column makes it difficult for SCS to target certain regions of the body (e.g. the bladder, feet), and has contributed to the limited success of SCS in treating focal pain etiologies (Kumar et al. 2011). Furthermore, the presence of highly conductive cerebrospinal fluid (CSF) around the spinal cord can shunt electrical current away from the targeted region (Holsheimer 2002). SCS leads are prone to migration over time, and changes in posture can affect the position of the spinal cord relative to the electrode lead, both of which further affect the accurate delivery of electrical stimulation to the spinal cord (Lempka and Patil 2018). With these shortcomings in mind, DRGS was developed to provide a new therapy for patients with refractory focal pain.

In contrast to SCS, DRGS is achieved by implanting a cylindrical stimulating electrode in the intraforaminal epidural space above a dorsal root ganglion (DRG). Due to the compactness of the intraforaminal space and scarcity of CSF around the ganglion (Brierley 1950), DRGS electrode leads consistently remain in close proximity to the DRG without much migration, and are less prone to the postural effects that hamper SCS leads (Kramer et al. 2015). Since a DRG innervates a single dermatome of the body, electrical stimulation of a DRG could provide dermatome-specific pain relief, suggesting that DRGS may be effective for patients with pain that is difficult to target with conventional SCS (e.g. bladder pain, focal foot pain). DRGS was approved by the Food and Drug Administration in 2016 to treat intractable complex regional pain syndrome (CRPS) of the lower limbs (Deer and Pope 2016), and has been used off-label for several other pain etiologies (e.g. phantom limb pain, painful diabetic neuropathy, groin pain) (Schu et al. 2014; Eldabe et al. 2015, 2018; Mol and Roumen 2018). Though preliminary clinical studies report success in many patients (approximately 75%) (Deer et al. 2017), not all patients receive adequate pain relief from DRGS. One contributing factor to the limited success rate of DRGS is that we do not understand the mechanisms of action by which DRGS provides pain relief. Without a mechanistic understanding of DRGS, we cannot optimize clinical parameters (e.g. stimulation amplitude, electrode lead position) to maximize pain relief in all patients.

The DRG is a bulge in the posterior spinal root, located bilaterally in the intraforaminal space at each spinal vertebral level. Each DRG contains the cell bodies of all the primary sensory neurons (PSNs) innervating the dermatome governed by its spinal segmental level (e.g. the left L5 DRG innervates the left foot). PSNs are pseudounipolar – the soma has a single axon process (the stem axon) that bifurcates at a large node of Ranvier called the T-junction. One axon projects centrally and terminates in the spinal cord, while the other projects to the periphery and terminates in a nerve ending (Ha 1970; Spencer et al. 1973; Devor 1999). Two types of PSNs commonly examined in pain pathophysiology studies are the large myelinated Aβ-fiber and the small nonmyelinated C-fiber (Devor 1999, 2009; Djouhri et al. 2006). Aβ-fibers typically convey innocuous tactile stimuli, but have been shown to generate ectopic action potentials (APs) in some chronic pain models, and are known to contribute to the development of tactile allodynia (Campbell et al. 1988; Kajander and Bennett 1992; Liu et al. 2000b; Devor 2009; Kovalsky et al. 2009; Prescott et al. 2014). C-fibers typically convey noxious stimuli. In some chronic pain conditions, peripheral sensitization of C-fibers may generate aberrant action potentials at the site of a neuroma or tissue damage (Blumberg and Jänig 1984; Welk et al. 1990; Liu et al. 2000b, 2000a). The importance of the DRG in the development and maintenance of chronic pain is well understood, making it an attractive target for neurostimulation therapies. However, our limited understanding of the therapeutic mechanisms of DRGS precludes the design of stimulation technologies (e.g. stimulus waveforms, electrode designs) to take full advantage of these mechanisms.

To understand the mechanisms of DRGS, it is imperative to first understand which neural elements are directly modulated by DRGS. Currently, there are several hypotheses to explain the therapeutic mechanisms of DRGS, ranging from filtering nociceptive impulses before they reach the spinal cord, to suppressing aberrant electrical activity of PSNs (Azeem and Attias 2018). However, there is no clinical evidence directly supporting any one hypothesis. *In-vitro* studies have shown that C-type fibers exhibit a low-pass filtering effect at the T-junction that prevents some peripherally-generated noxious afferent signals from reaching the central axon branch leading to the spinal cord. These studies also suggest that extracellular electrical stimulation can enhance this filtering effect (Gemes et al. 2013; Koopmeiners et al. 2013). The only previously-published computer modeling study of DRGS showed that clinical DRGS may provide pain relief by augmenting this mechanism (Kent et al. 2018). However, the stimulation amplitudes required to produce filtering (approximately 9.5 mA) were far outside clinical ranges (typically $\leq$ 1mA) (Deer et al. 2017), suggesting that DRGS provides pain relief through other mechanisms in clinical contexts. It is well understood that extracellular stimulation preferentially activates large-diameter myelinated axons over small nonmyelinated axons (Rattay 1986) and this trend suggests that Aβ-fibers and not C-fibers may be directly stimulated by DRGS.

In this work, we developed a computer model of clinical DRGS to investigate the mechanisms by which DRGS provides pain relief. We developed a volume conductor model of a human L5 DRG, a common stimulation target to manage chronic foot pain (Bendinger and Plunkett 2015; Eldabe et al. 2015, 2018). We coupled this anatomical model to multi-compartment models of Aβ- and C-fibers. We validated these cell models against experimental data. We developed the first computer model examining the effects of DRGS on both myelinated and nonmyelinated afferents, and showed that at stimulation amplitudes within typical clinical ranges, electrical stimulation is driving the activity of Aβ-fibers but not activating C-fibers. These results suggest that DRGS may provide pain relief by activating pain-gating mechanisms within the dorsal horn. Lastly, we examined the effect of electrode location on DRGS-induced neural activation, and suggest that straddling the active and return electrodes over the ganglion may be the optimal electrode configuration for activating neural tissue.

2. Methods

We developed computer models to investigate how DRGS affects sensory neurons in the DRG. We coupled multi-compartment models of primary sensory neurons to a three-dimensional finite element model (FEM) of a human L5 DRG. We calculated the voltage distribution generated by DRGS throughout the DRG and surrounding anatomy. We applied these voltages to the multi-compartment models of sensory neurons within the DRG, and examined how different sensory neuron types (i.e. mechanoreceptors and nociceptors) responded to DRGS.

2.1. Step 1: Calculate the extracellular voltages generated by DRGS

We constructed a three-dimensional FEM based on experimentally measured values to create an anatomically- and electrically-accurate volume conductor model of a human L5 DRG (Figure 1 and Table 1). The geometry of the model was based on published cadaver and imaging studies of the DRG and surrounding anatomy (e.g. dural covering, intraforaminal tissue, bone) (Hasegawa et al. 1996; Hogan 1996; Reina et al. 2007; Silverstein et al. 2015). The electrical conductivity of each tissue was based on values used in previous computational studies of neurostimulation for pain, and experimentally-measured tissue resistivities (Geddes and Baker 1967; Grill and Mortimer 1994; Gabriel et al. 1996; Lempka et al. 2015). Each conductivity was modeled as isotropic, except the nerve root, which was two-dimensionally anisotropic white matter (Table 2). The FEM was built in the commercially-available software 3-matic Module within the Mimics Innovation Suite (Materialise, Belgium). We included a model of the four-contact Abbott Axium™ DRG electrode array (Abbott Laboratories, USA) oriented above the DRG such that the active electrode was centered directly above the middle of the ganglion. We wanted to examine the effect of electrode lead position on neural activation. Therefore, in some simulations (where noted below) we shifted the electrode so that the active and return electrodes straddled the DRG such that the halfway point between the middle of the two electrodes was directly above the middle of the ganglion. We shifted the electrode 3.125 mm along the nerve root (i.e. half of the distance from the middle of one contact to the middle of an adjacent contact). We encased the electrode in a 300-μm thick encapsulation layer to represent the typical foreign body response to implanted materials (Grill and Mortimer 1994).

We imported the FEM into COMSOL Multiphysics (COMSOL, Inc., USA). Clinically, DRGS utilizes a bipolar electrode configuration (Kramer et al. 2015). To model bipolar DRGS, we applied boundary conditions at the active electrode (i.e. current stimulation) and the return electrode (i.e. ground; 0 V). We modeled the electrode shaft as a perfect insulator. We modeled inactive electrode contacts as equipotential with zero net current across their surface. To model DRGS, we calculated the voltage distribution generated by a unitary stimulus current (i.e. 1A) using the conjugate gradient method to solve the Poisson equation:

$$\nabla(\sigma\nabla\Phi) = -I \qquad (1)$$

where I is the applied current, σ is the tissue stiffness matrix, and Φ are the calculated voltage distributions. We used Ohm's law to calculate the impedance of the bipolar stimulation configurations by measuring the average voltage generated at the active electrode and dividing by the applied stimulus current. We then compared our average model impedances to clinically-measured impedances. The model's average impedance (1500 Ω) was within clinically-reported impedance ranges (Deer et al. 2019).

2.2. Step 2: Define sensory neuron models in the DRG

We used the freely-available software package, NEURON (v7.4) (Hines and Carnevale 1997), to construct all multi-compartment models of primary sensory neurons described below.

2.2.1. Aβ-fiber model

We developed a model of an Aβ-fiber (Figure 2) based on morphological parameters from previous studies (Table 3) (Ito and Takahashi 1960; Amir and Devor 2003). We extended a model of a mammalian axon – the MRG model (McIntyre et al. 2002) – to describe the pseudounipolar morphology of Aβ-fibers. The MRG model is a double-cable model of a mammalian motor axon with nodes of Ranvier separated by three distinct finite impedance myelin segments: the myelin attachment segment, a paranode main segment, and internode regions. We accounted for two features of Aβ-fiber internode regions not accounted for in the original MRG model (Figure 2): 1) the internode regions of the stem axon become increasingly myelinated near the bifurcation node, and 2) the first several internodes of the central and peripheral axons increase in length moving distally from the T-junction until they reach a consistent value (Amir and Devor 2003). The spinal axons of PSNs are smaller in diameter than the peripheral axons (Ha 1970). Therefore, we set our Aβ-fiber model central axon diameter to 5.7 μm and the peripheral axon diameter to 7.3 μm (Lee et al. 1986). The myelinated compartments were made of two concentric layers containing linear leak conductances with a parallel membrane capacitance. The nodes of Ranvier contained the parallel active nodal conductances of the sensory-specific axons described by (Gaines et al. 2018): fast Na^+, persistent Na^+, fast K^+, and slow K^+ ion channels. The active nodal conductances were in parallel with a linear leakage conductance and membrane capacitance (Table 3). We increased the model's leak conductance from 6 to 8 mS/cm^2 to reduce membrane potential fluctuation at simulation onset. We increased the slow K^+ channel's β rate constant's *A* parameter from 0.03 to 0.06 ms^{-1} to better fit the experimental values of AHP amplitude and duration (Harper and Lawson 1985b; Villière and McLachlan 1996). The soma and initial segment contained the same active ion channels as the nodes, but with sodium channel densities of 300 channels/μm^2 and 500 channels/μm^2, respectively (Matsumoto and Rosenbluth 1985). Note that we used an initial segment channel density of 500 channels/μm^2, which is slightly lower than the ~800 particles/μm^2 reported in (Matsumoto and Rosenbluth 1985), but was necessary to prevent the cell from generating spontaneous action potentials at the initial segment. We believe this is a reasonable modification, as the Aβ-fiber model reproduced many action potential characteristics seen in literature (Table 4).

2.2.2. C-fiber model

We implemented a model of a nonmyelinated C-fiber (Figure 2 and Table 3) based on morphological values described by (Sundt et al. 2015). The C-fiber membrane contained active conductances commonly seen in C-type nociceptors, and are studied as targets in pharmacological pain treatment. Specifically, we implemented the active ion channels and corresponding channel densities described in (Sheets et al. 2007): TTX-Sensitive $Na_v1.7$, TTX-Resistant $Na_v1.8$, a delayed rectifier K^+ channel, and a transient A-type K^+ channel. We also included the slow TTX-Resistant $Na_v1.9$ from (Huang et al. 2014). We included a passive leak channel with a conductance set to balance the resting membrane potential at -55 mV (Sundt et al. 2015). All compartments contained equal distributions of each ion channel type, as nonmyelinated axons have largely homogeneous membrane structures (Waxman and Ritchie 1985). To reduce computational demand while still ensuring model accuracy, we set the compartment lengths in the peripheral and spinal axons to 10 μm (Kent et al. 2018) for compartments within 20 mm of the bifurcation point (i.e. near the stimulating electrode) and 500 μm elsewhere along the axon. The stem axon was divided into 100 compartments of equal length (8.4 μm) (Sundt et al. 2015). The C-fiber model matched well with experimental somatic action potential values (Table 4).

2.2.3. Spontaneously active fibers

In a subset of simulations, we modified the Aβ-fiber and C-fiber models to produce spontaneous activity – a feature of some chronic pain states – to examine how DRGS affects pain-state sensory neurons. Aβ-fibers fire ectopic action potentials generated in the soma in some models of chronic pain (Campbell et al. 1988; Amir et al. 2002, 2005; Devor 2009; Kovalsky et al. 2009). This phenomenon is mediated in part by a decrease in somatic potassium conductance (Xiao et al. 2002; Dawes et al. 2018; Hunt et al. 2018), and an increase in sodium conductance (Ishikawa et al. 1999; Waxman 1999; Devor 2006). We therefore decreased somatic potassium conductance by 20% (Dawes et al. 2018) and increased sodium conductance by 50% so the model generated ectopic action potentials in the soma at frequencies reported in experimental studies (28 Hz) (Kajander and Bennett 1992; Amir et al. 2005).

C-fibers rarely generate ectopic APs in their somata (Devor et al. 1985; Song et al. 1999; Liu et al. 2000b; Amir et al. 2002). Instead, pain-state C-fiber activity often arises as aberrant signals coming from the periphery, usually at the site of tissue damage (e.g. neuroma, inflammation) (Blumberg and Jänig 1984; Welk et al. 1990; Liu et al. 2000b, 2000a). Therefore, we modeled pain-state C-fibers by introducing synaptic events in the peripheral axon to simulate painful APs generated in painful tissue (NEURON's NetStim class, 50 ms spike period).

We next placed the sensory neurons models within the DRG. A recent study showed that in mammalian DRG, cell bodies are preferentially located around the dorsal edge of the ganglion (Ostrowski et al. 2017), but the spatial distribution of Aβ- and C-fibers within the DRG is unknown. Therefore, we homogeneously distributed each cell type throughout the DRG. We placed the somata of both sensory neuron models on a 2D regular grid within the sagittal and transverse planes of the DRG (Figure 3A; Figure 4A, gray shaded areas) with 100 μm spacing in all directions. Stem axons projected towards the midline of the ganglion, then bifurcated into central and peripheral processes that curved ventrally to enter the nerve root. The stem axon and soma totaled 869 μm in length for both cell models (Amir and Devor 2003). Figures 1 and 3 show an example axon trajectory within the FEM.

2.3. Step 3: Determine the cellular response to DRGS

We interpolated the extracellular voltages calculated from the FEM (equation 1) onto the center of each neuron compartment. We used the NEURON simulation environment (v7.4) within the Python programming language (Hines and Carnevale 1997; Hines et al. 2009) to apply the extracellular voltages to both cell models using NEURON's extracellular mechanism. For each simulation, we calculated each neural compartment's time-varying membrane potential, V_m, by using a backward Euler implicit integration method with a time step of 0.005 ms to solve the cable equation:

$$r_i c_m \frac{\partial V_m}{\partial t} = \frac{\partial^2 V_m}{\partial x^2} + \frac{\partial^2 V_e}{\partial x^2} - \frac{r_i}{r_m} \sum I_{ion} \tag{2}$$

where r_m is the membrane resistance, r_i is the intracellular resistance, V_e is the extracellular potential, and c_m is the membrane capacitance. The $\sum I_{ion}$ term represents the sum of all ionic currents through a given compartment. The ionic current for a generic ion (e.g. sodium, potassium) is represented by the Hodgkin-Huxley formalism:

$$I_{ion} = \bar{g}_{ion} s (V_m - E_{ion}) \tag{3}$$

where $\bar{g}_{ion}$ is the maximal ionic conductance, s is a state variable, and E_{ion} is the ionic reversal potential. Some ionic currents have more than one state variable. For the full formulation of each ion channel's current equation, we refer the reader to their original manuscripts (Sheets et al. 2007; Huang et al. 2014; Gaines et al. 2018). Because the FEM tissue conductivities were linear, the voltage distribution generated by a given stimulus amplitude was a scalar multiple of the voltage distribution generated by a unit stimulus (i.e. a 1 A stimulus) (Moffitt and McIntyre 2005).

We examined sensory neuron response to DRGS (Figure 3). We calculated the minimum stimulation amplitude to elicit one or more action potentials (i.e. the activation threshold) in both fiber types. All pulses were biphasic with a stimulus pulse followed by a passive discharge phase. To mimic common parameter values used in clinical DRGS, we used a stimulus pulse width of 300 μs, an interphase interval of 20 μs (i.e. delay between the end of a stimulus pulse and the start of the passive discharge phase), and a pulse frequency of 40 Hz (Deer et al. 2017; Kent et al. 2018; Lempka et al. 2018). We calculated activation thresholds for both anodic- and cathodic-first stimulus pulses. We used a binary search algorithm to find the activation thresholds to within 0.1 μA.

3. Results

3.1 Cell model validation

We created multi-compartment models of two types of sensory neurons that are important in pain processing: a myelinated Aβ-fiber and a nonmyelinated C-fiber. Both the Aβ-fiber and C-fiber models reproduced somatic action potential characteristics observed in experimental studies (Huxley and Stämpfli 1951; Harper and Lawson 1985b; Villière and McLachlan 1996; Djouhri et al. 1998; Zhang et al. 1998; Amir and Devor 2003; Amir et al. 2005; Howells et al. 2012). The Aβ-fiber model matched experimental ranges of AP amplitude, AP duration, AHP amplitude, AHP half duration, resting membrane potential, and conduction velocity (CV). The C-fiber model matched experimental ranges of AP amplitude, AP duration, rise time, fall time, AHP amplitude, AHP half duration, resting membrane potential, and CV. The action potential rise and fall times of the Aβ-fiber model were slightly outside of the experimental range, however the total duration of the action potential matched experimental data. Table 4 summarizes the somatic action potential characteristics of our models and how they compared to values reported in literature.

3.2. Activation thresholds

DRG contain several types of primary sensory neurons that convey different sensory modalities (e.g. touch, pain). Large myelinated fibers, such as Aβ-fibers, typically convey innocuous touch stimuli, while small nonmyelinated fibers, such as C-fibers, typically convey noxious stimuli (Devor 1999). We wanted to determine which types of sensory neurons are likely being activated by DRGS. Therefore, we calculated the stimulation amplitudes necessary to elicit one or more action potentials in the multi-compartment models of Aβ- and C-fibers.

In Aβ-fibers, cathodic and anodic DRGS typically caused APs to initiate in either the peripheral or central axon – whichever was closer to the cathode. In C-fibers, most APs initiated in the stem axon when the cell body was near the anode, while APs were typically generated in the soma when the cell body was near the cathode. Figure 4B shows contour plots of the activation thresholds for Aβ- and C-fibers. Aβ-fiber thresholds were lower than C-fiber thresholds. Anodic thresholds were consistently lower than cathodic thresholds for both cell types. PSNs with cell bodies below an anode had lower thresholds than PSNs with cell bodies below a cathode. Activation thresholds increased with distance from the active and return electrodes. The minimum stimulation amplitude needed to elicit an action potential in an Aβ-fiber was 0.36 and 0.24 mA for cathodic and anodic DRGS, respectively. The minimum stimulation amplitude needed to elicit an action potential in a C-fiber was 4.38 and 4.09 mA for cathodic and anodic DRGS, respectively. On average, DRGS amplitudes used in clinical practice do not exceed 1 mA (Deer et al. 2017). With a 1 mA pulse amplitude, cathodic DRGS activated 29.5% of the modeled Aβ-fibers in the DRG, while anodic DRGS activated 74.6% of Aβ-fibers in our DRG model. Interestingly, there were no C-fibers activated within clinical amplitude ranges. These results suggest that, within clinical amplitudes, DRGS directly activated myelinated Aβ-fibers without activating nonmyelinated C-fibers.

3.3. DRGS drives regular firing of Aβ-fibers

Primary sensory neurons may go through quiescent periods in which they do not fire action potentials (e.g. when they do not receive sensory input). PSNs may also experience periods of spontaneous activity, such as in response to sensory stimuli or in some chronic pain states. Currently, we do not know how DRGS modulates the activity of sensory neurons in either state to provide analgesia. One theory suggests that DRGS provides analgesia by suppressing PSN hyperexcitability, or otherwise silencing abnormal electrical patterns of DRG neurons brought about by chronic pain (Azeem and Attias 2018). Conversely, the gate control theory of pain suggests that stimulation-induced pain relief is achieved by repeatedly activating large myelinated somatosensory fibers, activating inhibitory interneurons in the dorsal horn that silence transmission neurons (Melzack and Wall 1965; Braz et al. 2014).

We tested these theories by examining how DRGS modulates PSN activity under quiescent and spontaneously-active conditions. We implemented a pain-state model of an Aβ-fiber that generates ectopic action potentials from its soma (a feature of tactile allodynia) (Devor 2009), and a pain-state model of a C-fiber that generates action potentials in the peripheral axon (e.g. in response to tissue damage). We then applied suprathreshold clinical DRGS (0.75 mA pulse amplitude, 300 μs pulse width, 40 Hz pulse frequency) to examine the effect of stimulation on quiescent and spontaneously active fibers (Figure 5). Stimulating both quiescent and spontaneously active Aβ-fibers caused the fiber to fire one action potential in response to every stimulus pulse (i.e. one-to-one activation). DRGS did not elicit any action potentials in quiescent C-fibers. When stimulating spontaneously active C-fibers, DRGS did not suppress or drive activity. Instead, the cell continued to fire at its original frequency, and DRGS only evoked subthreshold responses. These results further suggest that clinical DRGS directly drives the activity of large myelinated Aβ-fibers without modulating C-fiber activity.

3.4. Effect of lead location

DRGS leads are implanted percutaneously, and guided into the intraforaminal space above the DRG (Vancamp et al. 2017). Clinicians use fluoroscopic imaging to visualize lead location during implantation, but fluoroscopy cannot resolve neural tissue. Therefore, the position of active and return electrodes relative to the DRG is difficult to ascertain during implantation. With variations in patient anatomy, it is possible that electrode location with respect to the ganglion is inconsistent across patients, and could potentially lead to differences in patient outcomes. We examined the effect of electrode position on PSN activation thresholds to determine how lead placement altered neural activation.

After shifting the electrode along the nerve root 3.125 mm (i.e. half the distance from the middle of one contact to the middle of an adjacent contact) so that the active and return electrodes straddled the ganglion, cathodic and anodic DRGS again caused APs to typically initiate in the axon closest to the cathode for Aβ-fibers. For both cathodic and anodic DRGS, C-fiber APs usually initiated in the soma when the cell body was below a cathode, and the stem axon when the cell body was below an anode. When the cell body was halfway between the anode and cathode, C-fiber APs were generated in either the peripheral or central axon. Figure 6B shows the activation thresholds for Aβ- and C-fibers when the active and return electrodes straddled the DRG. With the active and return electrodes straddling the ganglion, most cathodic thresholds were lower than anodic thresholds. The minimum amplitudes needed to elicit an action potential in an Aβ-fiber was 0.27 and

0.34 mA for cathodic and anodic DRGS, respectively. The minimum amplitude to elicit an action potential in a C-fiber was 8.51 and 6.72 mA for cathodic and anodic DRGS, respectively. For Aβ-fibers, slightly fewer cells had anodic activation thresholds within clinical ranges when the active and return electrodes straddled the ganglion compared to when the active electrode is centered over the ganglion: 72.4% of cells vs 74.6% of cells, respectively. However, there were more Aβ-fibers with cathodic activation thresholds within clinical ranges when the active and return electrodes straddled the ganglion compared to the active electrode centered over the ganglion: 86.6% of cells vs. 29.5%, respectively. Straddling the active and return electrodes across the ganglion did not produce any C-fiber activation within clinical ranges. These results indicate that both stimulus polarity and the positioning of anodes and cathodes relative to the ganglia may alter the number of neurons activated by DRGS.

4. Discussion

DRGS is a promising therapy for chronic intractable pain. However, not all patients receive sufficient pain relief from DRGS. There are several factors that may contribute to these shortcomings, such as inconsistencies in lead positioning, stimulation parameter selection, and possible differences in mechanisms of action of chronic pain between different pain etiologies. Another likely contributing factor is that the physiological mechanisms of stimulation-induced pain relief are unknown. This knowledge gap prevents the design of stimulation therapies to specifically target these mechanisms. Uncovering these physiological mechanisms will be essential in maximizing pain relief in all patient populations. The data presented in this study are an important next step towards this goal. Our results suggest that within the range of clinical stimulation parameters, DRGS activates large myelinated Aβ-fibers but not small nonmyelinated C-fibers. Therefore, we conclude that a primary mechanism of DRGS-induced pain relief may be the activation of pain-gating mechanisms in the dorsal horn. Furthermore, our data suggest that cathodic DRGS applied with the active and return electrodes straddling the ganglion may activate more Aβ-fibers than other electrode configurations.

4.1. Potential mechanism of clinical DRGS

We employed a computer modeling approach to study the mechanisms of DRGS on PSNs. DRG contain several types of sensory neurons: large myelinated proprioceptive and mechanoreceptive fibers (e.g. Aβ-fibers), small thinly-myelinated mechanoreceptive, thermoceptive, and nociceptive fibers (e.g. Aδ-fibers), and small nonmyelinated mechanoreceptive and nociceptive fibers (e.g. C-fibers). In our model, we considered two sensory neurons commonly studied in chronic pain – the large myelinated mechanoreceptive Aβ-fiber, and the small nonmyelinated nociceptive C-fiber. Our results suggest that DRGS within clinical ranges of stimulation parameters (e.g. amplitude, pulse width) are directly activating Aβ-fibers, but not C-fibers (Figure 4). We observed this result irrespective of lead placement and stimulation configuration (Figure 6). DRGS caused one-to-one activation of Aβ-fibers, regardless of the fiber's activity before DRGS was turned on (Figure

5). Repeated activation of large myelinated Aβ-fibers suggests that DRGS may provide pain relief by activating pain-gating mechanisms within the spinal cord (Melzack and Wall 1965). This aligns well with the current theories on the mechanisms of action of SCS for pain, where SCS activates the large myelinated Aβ-fibers of the dorsal columns, which activate inhibitory interneurons in the dorsal horn (Holsheimer 2002; Guan 2012; Lempka and Patil 2018).

A recent computational study of DRGS examined the effect of stimulation on C-fibers (Kent et al. 2018). Kent and colleagues showed that DRGS activates C-fibers with stimulation amplitudes on the order of several milliamps, similar to the ranges reported in this study. We also corroborated their finding that action potentials typically initiate around the soma or stem axon in C-fibers. Their results suggest that DRGS could potentially generate analgesia by blocking painful afferent signals from propagating into the spinal axon by enhancing low-pass filtering of noxious afferent signals at C-fiber T-junctions. However, the stimulation amplitudes reported to elicit sustained block were far outside clinical ranges (> 9.5 mA). Therefore, we believe that in clinical scenarios, T-junction filtering is unlikely to be the primary mechanism of DRGS-induced pain relief, though it is likely important in normal physiologic pain processing (Gemes et al. 2013; Koopmeiners et al. 2013). Instead, our results suggest that DRGS within clinical parameter ranges directly activates large myelinated afferent fibers.

In this work, we used a computer model to examine the direct effects of DRGS on primary sensory neurons within the DRG. However, more work is needed to fully elucidate the pain-relief mechanisms of DRGS, particularly the downstream effects of stimulation. Recent studies have provided insight into the complexity of the spinal networks that govern pain transmission, highlighting that Aβ-afferents synapse onto both excitatory and inhibitory interneurons in the dorsal horn, which mediate the activity of projection neurons that carry sensory signals to the brain (Duan et al. 2014, 2018; Cheng et al. 2017). It is currently unknown: 1) how different chronic pain etiologies sensitize or disinhibit the various components of this network, 2) how the prolonged driving of Aβ-fiber activity with DRGS may induce changes in this network, 3) how Aβ-fiber and dorsal horn network response to stimulation may change in response to chronic DRGS, and 4) how long-term DRGS-induced changes in network dynamics vary between chronic pain etiologies. Experiments designed to answer these questions may provide insight into which pain etiologies are likely to receive therapeutic benefit from DRGS (Harrison et al. 2018), and why the therapeutic efficacy of DRGS appears to decrease over time (Eldabe et al. 2015; Morgalla et al. 2018). Furthermore, the results of those studies may inform the design of future computer models of DRGS to examine the effects of DRGS on dorsal horn circuitry. Such models could be used to optimize stimulation parameters to provide maximal pain relief.

4.2. Effect of electrode lead placement on neural activation

Because x-ray fluoroscopy cannot resolve neural tissue, it is difficult to determine the position of DRGS electrodes relative to the ganglion during implantation. It is possible that electrode placement with respect to the ganglion could be variable across patients, which may be a factor in the limited success of DRGS. To determine how this may affect the neural activation produced by DRGS, we examined the effect of lead position relative to the ganglion on DRGS-induced neural activation (Figure 6). We showed that regardless of lead position, clinical DRGS activates Aβ-fibers but not C-fibers. When the active and return electrodes straddled the ganglion, cathodic DRGS activated significantly more Aβ-fibers than when the active electrode was centered above the ganglion (86.6% and 29.5% of Aβ-fibers within the ganglion, respectively). This result is likely due to the cathode being closer to the nerve root, which contains the axons of PSNs but not cell bodies. It is well understood that cathodic extracellular stimulation has lower thresholds when the cathode is near an axon compared to near a cell body (Ranck 1975; McIntyre and Grill 1999). Interestingly, when the active and return electrodes straddled the ganglion, the number of cells activated by clinical ranges of anodic DRGS only decreased by 2.2%, possibly because the active electrode remained close enough to the ganglion to directly stimulate cells with somata around the dorsal edge of the ganglion.

These results suggest that if DRGS provides pain relief by activating Aβ-fibers, the optimal stimulation parameters may be to have the active and return electrodes straddle the DRG and to apply cathodic DRGS. This is consistent with previous clinical reports that suggested straddling the second and third electrodes across the pedicle was the ideal electrode lead location (Eldabe et al. 2015). Lumbar ganglia are typically located under the pedicle in the 'foraminal region,' suggesting that electrode location with respect to the pedicle may be a good proxy for electrode location with respect to the ganglia at those levels (Kikuchi et al. 1994; Hasegawa et al. 1996; Silverstein et al. 2015).

Our model suggests that a straddled electrode configuration would activate the largest number of Aβ-fibers for a given stimulation amplitude, thus minimizing power consumption. It is important to note that our model assumed a homogeneous distribution of each afferent type throughout the DRG, while the spatial distribution of different types of PSNs in human DRG is unknown. Previous studies in rats suggest that two-thirds of L5 DRG neurons are C-type fibers (Tandrup 1993), and that lumbar DRG may show digit-specific organization (Prats-Galino et al. 1999). However, it is unclear if DRG neurons also organize based on sensory modality, though it has been suggested (Puigdellívol-Sánchez et al. 1998). Deciphering the location of Aβ-fibers within human DRG may inform the ideal location in which to place the electrode lead to effectively target these populations.

4.3. Limitations

We used a computer model to investigate which cells are directly stimulated by DRGS. Computer modeling has been a powerful tool in understanding the mechanisms of action of other neurostimulation therapies, such as deep brain stimulation (McIntyre et al. 2004b) and SCS (Struijk et al. 1992, 1993). However, it will be imperative to confirm our findings with experimental data, and to use those data to validate and refine our model design. Furthermore, there are several limitations to our approach with regards to studying DRGS-induced pain relief. First, we examined only two sensory neurons found within human DRG: Aβ- and C-fibers. Though Aβ-fibers and C-fibers are crucial in the development and maintenance of chronic pain, other cell types, such as Aα-proprioceptors and Aδ-thermoceptors and nociceptors, may also play important roles (Devor

1999). In particular, Aδ-fibers are of interest, as Aδ-fibers typically convey thermal or mechanical pain (Lawson 2005; Todd 2010; Hu et al. 2014). Since Aδ-fibers are myelinated, albeit thinly, it is possible that DRGS will directly affect their firing patterns compared to the nonmyelinated C-fibers. However, we excluded these fibers from our analyses because of a paucity of experimental data necessary to describe Aδ-fiber ion channel physiology. Because Aδ-fibers are known to play an important role in several forms of chronic pain (Kajander and Bennett 1992; Todd 2010; Hu et al. 2014), future computational modeling studies should consider the effects of DRGS on Aδ-fibers.

We made several simplifications with regards to the ion channels included in our multi-compartment sensory neuron models. Sensory neurons express a myriad of ion channels, but due to computational demands and limited experimental data, it is not possible to model every ion channel type present in sensory neurons. Therefore, we focused on the major ion channels necessary to reproduce the somatic action potential characteristics described in previous experimental studies. Future DRGS studies could consider a more complete model of PSN ion channel physiology, particularly with regards to the long-term effects of stimulation (e.g. calcium sequestration, synaptic transmitter release).

We developed a simplified representation of a human DRG using a cylindrical volume conductor model, a similar approach used previously to study the mechanisms of action of neurostimulation therapies (McIntyre et al. 2004a; Datta et al. 2008; Lempka et al. 2015). We assumed an idealized trajectory for axons within the ganglion. In our models, stem axons projected towards the midline of the ganglion and nerve root, then bifurcated into central and peripheral axons which curved ventrally before entering the nerve root and following straight trajectories. In reality, stem axons are complex and winding, forming tightly packed glomeruli around somata before reaching bifurcating nodes (Devor 1999). The impact of tightly coiled stem axons on DRGS thresholds is currently unclear. Future studies should examine the effects of complex stem axon trajectories on neuronal activation, and the extent to which ephaptic phenomena may influence DRGS outcomes.

5. Conclusions

DRGS is a promising therapy for chronic intractable pain. We examined which cell types in the DRG are directly stimulated by DRGS within clinical ranges of stimulation parameters. The results of this study suggest that large myelinated PSNs are directly driven by DRGS, indicating that DRGS-induced analgesia may be achieved by activating pain-gating mechanisms in the dorsal horn. We demonstrated that the position of the active and return electrodes can influence neural activation. Our results suggest that cathodic DRGS applied when the active and return electrodes straddle the ganglia activates more large myelinated afferents than electrodes placed over the medial aspect of the DRG.

References

Amir R, Devor M. Electrical excitability of the soma of sensory neurons is required for spike invasion of the soma, but not for through-conduction. Biophys J. 2003 Apr;84(4):2181–91.

Amir R, Kocsis JD, Devor M. Multiple interacting sites of ectopic spike electrogenesis in primary sensory neurons. J Neurosci. 2005;25(10):2576–85.

Amir R, Liu CN, Kocsis JD, Devor M. Oscillatory mechanism in primary sensory neurones. Brain. 2002;125(2):421–35.

Amirdelfan K, Kramer J, Cusack WF, Burton AW. Advanced neuromodulation techniques: Dorsal root ganglion stimulation. In: Advanced procedures for pain management: A step-by-step atlas. Springer International Publishing; 2018. p. 265–79.

Azeem N, Attias MD. Neuromodulation: Mechanisms of action. In: Advanced procedures for pain management: A step-by-step atlas. Springer International Publishing; 2018. p. 93–103.

Bendinger T, Plunkett N. Dorsal root ganglion stimulation vs. conventional spinal cord stimulation - efficacy and patient experience of two neurostimulation methods for the treatment of Complex Regional Pain Syndrome type II: A case report. J Obs Pain Med. 2015;1(5):42–7.

Blumberg H, Jänig W. Discharge pattern of afferent fibers from a neuroma. Pain. 1984;20(4):335–53.

Braz J, Solorzano C, Wang X, Basbaum A. Transmitting pain and itch messages: A contemporary view of the spinal cord circuits that generate gate control. Neuron. 2014;82(3):522–36.

Brierley JB. The penetration of particulate matter from the cerebrospinal fluid into the spinal ganglia, peripheral nerves, and the perivascular spaces of the central nervous system. J Neurol Neurosurg Psychiatry. 1950;13(3):203–15.

Campbell JN, Raja SN, Meyer RA, Mackinnon SE. Myelinated afferents signal the hyperalgesia associated with nerve injury. Pain. 1988;32(1):89–94.

Cheng L, Duan B, Huang T, Zhang Y, Chen Y, Britz O, et al. Identification of spinal circuits involved in touch-evoked dynamic mechanical pain. Nat Neurosci. 2017;20(6):804–14.

Datta A, Elwassif M, Battaglia F, Bikson M. Transcranial current stimulation focality using disc and ring electrode configurations: FEM analysis. J Neural Eng. 2008;5(2):163–74.

Dawes JM, Weir GA, Middleton SJ, Patel R, Chisholm KI, Pettingill P, et al. Immune or genetic-mediated disruption of CASPR2 causes pain hypersensitivity due to enhanced primary afferent excitability. Neuron. 2018;97(4):806–22.

Deer TR, Levy RM, Kramer J, Poree L, Amirdelfan K, Grigsby E, et al. Dorsal root ganglion stimulation yielded higher treatment success rate for CRPS and causalgia at 3 and 12 months. Pain. 2017;158(4):669–81.

Deer TR, Pope JE. Dorsal root ganglion stimulation approval by the Food and Drug Administration: Advice on evolving the process. Expert Rev Neurother. 2016;16(10):1123–5.

Deer TR, Pope JE, Lamer TJ, Grider JS, Provenzano D, Lubenow TR, et al. The Neuromodulation Appropriateness Consensus Committee on best practices for dorsal root ganglion stimulation. Neuromodulation. 2019;22(1):1–35.

Devor M. Unexplained peculiarities of the dorsal root ganglion. Pain. 1999;82(Supplement 6):S27–35.

Devor M. Sodium channels and mechanisms of neuropathic pain. J Pain. 2006;7(1S):S3–12.

Devor M. Ectopic discharge in Aβ afferents as a source of neuropathic pain. Exp Brain Res. 2009;196(1):115–28.

Devor M, Govrin-Lippmann R, Raber P. Corticosteroids suppress ectopic neural discharge originating in experimental neuromas. Pain. 1985;22(2):127–37.

Djouhri L, Bleazard L, Lawson SN. Association of somatic action potential shape with sensory receptive properties in guinea-pig dorsal root ganglion neurones. J Physiol. 1998;513(3):857–72.

Djouhri L, Koutsikou S, Fang X, McMullan S, Lawson SN. Spontaneous pain, both neuropathic and inflammatory, is related to frequency of spontaneous firing in intact C-fiber nociceptors. J Neurosci. 2006;26(4):1281–92.

Duan B, Cheng L, Bourane S, Britz O, Padilla C, Garcia-Campmany L, et al. Identification of spinal circuits transmitting and gating mechanical pain. Cell. 2014;159(6):1417–32.

Duan B, Cheng L, Ma Q. Spinal circuits transmitting mechanical pain and itch. Neurosci Bull. 2018;34(1):186–93.

Eldabe S, Burger K, Moser H, Klase D, Schu S, Wahlstedt A, et al. Dorsal root ganglion (DRG) stimulation in the treatment of phantom limb pain (PLP). Neuromodulation. 2015;18(7):610–7.

Eldabe S, Espinet A, Wahlstedt A, Kang P, Liem L, Patel NK, et al. Retrospective case series on the treatment of painful diabetic peripheral neuropathy with dorsal root ganglion stimulation. Neuromodulation. 2018;21(18):787–92.

Gabriel S, Lau RW, Gabriel C. The dielectric properties of biological tissues: III. Parametric models for the dielectric spectrum of tissues. Phys Med Biol. 1996;41(11):2271–93.

Gaines JL, Finn KE, Slopsema JP, Heyboer LA, Polasek KH. A model of motor and sensory axon activation in the median nerve using surface electrical stimulation. J Comput Neurosci. 2018;45(1):29–43.

Gaskin DJ, Richard P. The economic costs of pain in the United States. J Pain. 2012;13(8):715–24.

Geddes LA, Baker LE. The specific resistance of biological material - a compendium of data for the biomedical engineer and physiologist. Med Biol Eng. 1967;5(3):271–93.

Gemes G, Koopmeiners A, Rigaud M, Lirk P, Sapunar D, Bangaru ML, et al. Failure of action potential propagation in sensory neurons: Mechanisms and loss of afferent filtering in C-type units after painful nerve injury. J Physiol. 2013;591(4):1111–31.

Grill WM, Mortimer JT. Electrical properties of implant encapsulation tissue. Ann Biomed Eng. 1994;22(1):23–33.

Guan Y. Spinal cord stimulation: Neurophysiological and neurochemical mechanisms of action. Curr Pain Headache Rep. 2012;16(3):217–25.

Ha H. Axonal bifurcation in the dorsal root ganglion of the cat: A light and electron microscopic study. J Comp Neurol. 1970;140(2):227–40.

Harper AA, Lawson SN. Conduction velocity is related to morphological cell type in rat dorsal root ganglion neurones. J Physiol. 1985a;359(1):31–46.

Harper AA, Lawson SN. Electrical properties of rat dorsal root ganglion neurones with different peripheral nerve conduction velocities. J Physiol. 1985b;359(1):47–63.

Harrison C, Epton S, Bojanic S, Green AL, FitzGerald JJ. The efficacy and safety of dorsal root ganglion stimulation as a treatment for neuropathic pain: A literature review. Neuromodulation. 2018;21(3):225–33.

Hasegawa T, Mikawa Y, Watanabe R, An HS. Morphometric analysis of the lumbrosacral nerve roots and dorsal root ganglia by magnetic resonance imaging. Spine. 1996;21(9):1005–9.

Hines ML, Carnevale NT. The NEURON simulation environment. Neural Comput. 1997;9(6):1179–209.

Hines ML, Davison AP, Muller E. NEURON and python. Front Neuroinform. 2009;3(1):1–12.

Hogan Q. Size of human lower thoracic and lumbosacral nerve roots. Anesthesiology. 1996;85(1):37–42.

Holsheimer J. Which neuronal elements are activated directly by spinal cord stimulation. Neuromodulation. 2002;5(1):25–31.

Howells J, Trevillion L, Bostock H, Burke D. The voltage dependence of Ih in human myelinated axons. J Physiol. 2012;590(7):1625–40.

Hu L, Cai MM, Xiao P, Luo F, Iannetti GD. Human brain responses to concomitant stimulation of Aδ and C nociceptors. J Neurosci. 2014;34(34):11439–51.

Huang J, Han C, Estacion M, Vasylyev D, Hoeijmakers JGJ, Gerrits MM, et al. Gain-of-function mutations in sodium channel Nav1.9 in painful neuropathy. Brain. 2014;137(6):1627–42.

Hunt MA, Nascimento DSM, Bersellini Farinotti A, Svensson CI. Autoantibodies hurt: Transfer of patient-derived CASPR2 antibodies induces neuropathic pain in mice. Neuron. 2018;97(4):729–31.

Huxley AF, Stämpfli R. Direct determination of membrane resting potential and action potential in single myelinated nerve fibres. J Physiol. 1951;112(3–4):476–95.

Ishikawa K, Tanaka M, Black J a, Waxman SG. Changes in expression of voltage-gated potassium channels in dorsal root ganglion neurons following axotomy. Muscle Nerve. 1999;22(4):502–7.

Ito M, Takahashi I. Impulse conduction through spinal ganglion. In: Electrical Activity of Single Cells. 1960. p. 159–79.

Kajander KC, Bennett GJ. Onset of a painful peripheral neuropathy in rat: A partial and differential deafferentation and spontaneous discharge in Aβ and Aδ primary afferent neurons. J Neurophysiol. 1992;68(3):734–44.

Kent AR, Min X, Hogan QH, Kramer JM. Mechanisms of dorsal root ganglion stimulation in pain suppression: A computational modeling analysis. Neuromodulation. 2018;21(3):234–46.

Kikuchi S, Sato K, Konno S, Hasue M. Anatomic and radiographic study of dorsal root ganglia. Spine. 1994;19(1):6–11.

Koopmeiners AS, Mueller S, Kramer J, Hogan QH. Effect of electrical field stimulation on dorsal root ganglion neuronal function. Neuromodulation. 2013;16(4):304–11.

Kovalsky Y, Amir R, Devor M. Simulation in sensory neurons reveals a key role for delayed Na+ current in subthreshold oscillations and ectopic discharge: Implications for neuropathic pain. J Neurophysiol. 2009;102(3):1430–42.

Kramer J, Liem L, Russo M, Smet I, Van Buyten JP, Huygen F. Lack of body positional effects on paresthesias when stimulating the dorsal root ganglion (DRG) in the treatment of chronic pain. Neuromodulation. 2015;18(1):50–7.

Kumar K, Rizvi S, Bnurs SB. Spinal cord stimulation is effective in management of complex regional pain syndrome I: Fact or fiction. Neurosurgery. 2011;69(3):566–78.

Lawson SN. The peripheral sensory nervous system: Dorsal root ganglion neurons. In: Peripheral Neuropathy. Elsevier Inc.; 2005. p. 163–202.

Lee KH, Chung K, Chung JM, Coggeshall RE. Correlation of cell body size, axon size, and signal conduction velocity for individually labelled dorsal root ganglion cells in the cat. J Comp Neurol. 1986;243(3):335–46.

Lempka SF, Howell B, Gunalan K, Machado AG, McIntyre CC. Characterization of the stimulus waveforms generated by implantable pulse generators for deep brain stimulation. Clin Neurophysiol. 2018 Apr;129(4):731–42.

Lempka SF, McIntyre CC, Kilgore KL, Machado AG. Computational analysis of kilohertz frequency spinal cord stimulation for chronic pain management. Anesthesiology. 2015;122(6):1362–76.

Lempka SF, Patil PG. Innovations in spinal cord stimulation for pain. Curr Opin Biomed Eng. 2018;8:51–60.

Liu CN, Michaelis M, Amir R, Devor M. Spinal nerve injury enhances subthreshold membrane potential oscillations in DRG neurons: Relation to neuropathic pain. J Neurophysiol. 2000a;84(1):205–15.

Liu CN, Wall PD, Ben-Dor E, Michaelis M, Amir R, Devor M. Tactile allodynia in the absence of C-fiber activation: Altered firing properties of DRG neurons following spinal nerve injury. Pain. 2000b;85(3):503–21.

Matsumoto E, Rosenbluth J. Plasma membrane structure at the axon hillock, initial segment and cell body of frog dorsal root ganglion cells. J Neurocytol. 1985;14(5):731–47.

McIntyre CC, Grill WM. Excitation of central nervous system neurons by nonuniform electric fields. Biophys J. 1999;76(2):878–88.

McIntyre CC, Grill WM, Sherman DL, Thakor N V. Cellular effects of deep brain stimulation: Model-based analysis of activation and inhibition. J Neurophysiol. 2004a;91(4):1457–69.

McIntyre CC, Richardson AG, Grill WM. Modeling the excitability of mammalian nerve fibers: Influence of afterpotentials on the recovery cycle. J Neurophysiol. 2002;87(2):995–1006.

McIntyre CC, Savasta M, Kerkerian-Le Goff L, Vitek JL. Uncovering the mechanism(s) of action of deep brain stimulation: Activation, inhibition, or both. Clin Neurophysiol. 2004b;115(6):1239–48.

Melzack R, Wall PD. Pain mechanisms: A new theory. Science. 1965;150(3699):971–9.

Moffitt MA, McIntyre CC. Model-based analysis of cortical recording with silicon microelectrodes. Clin Neurophysiol. 2005;116(9):2240–50.

Mol FMU, Roumen RMH. DRG spinal cord stimulation as solution for patients with severe pain due to anterior cutaneous nerve entrapment syndrome: A case series. Neuromodulation. 2018;21(3):317–9.

Morgalla MH, Bolat A, Fortunato M, Lepski G, Chander BS. Dorsal root ganglion stimulation (DRGS) for the treatment of chronic neuropathic pain: A single-center study with long-term prospective results in 62 Cases. Pain Physician. 2018;21(4):E377–88.

Ostrowski AK, Sperry ZJ, Kulik G, Bruns TM. Quantitative models of feline lumbosacral dorsal root ganglia neuronal cell density. J Neurosci Methods. 2017;290:116–24.

Prats-Galino A, Puigdellívol-Sánchez A, Ruano-Gil D, Molander C. Representations of hindlimb digits in rat dorsal root ganglia. J Comp Neurol. 1999;408(1):137–45.

Prescott SA, Ma Q, De Koninck Y. Normal and abnormal coding of somatosensory stimuli causing pain. Nat Neurosci. 2014;17(2):183–91.

Puigdellívol-Sánchez A, Prats-Galino A, Ruano-Gil D, Molander C. Sciatic and femoral nerve sensory neurones occupy different regions of the L4 dorsal root ganglion in the adult rat. Neurosci Lett. 1998;251(3):169–72.

Ranck JB. Which elements are excited in electrical stimulation of mammalian central nervous system: A review. Brain Res. 1975;98(3):417–40.

Rattay F. Analysis of models for external stimulation of axons. IEEE Trans Biomed Eng. 1986;BME-33(10):974–7.

Reina MA, Villanueva MC, Lopez A, De Andres JA. Grasa dentro de los manguitos durales de las raices nerviosas de la columna lumbar humana. Rev Esp Anestesiol Reanim. 2007;54(5):297–301.

Schu S, Gulve A, Eldabe S, Baranidharan G, Wolf K, Demmel W, et al. Spinal cord stimulation of the dorsal root ganglion for groin pain - a retrospective review. Pain Pract. 2014;15(4):293–9.

Sheets PL, Jackson JO, Waxman SG, Dib-hajj SD, Cummins TR. A Nav 1.7 channel mutation associated with hereditary erythromelalgia contributes to neuronal hyperexcitability and displays reduced lidocaine sensitivity. J Physiol. 2007;581(3):1019–31.

Silverstein MP, Romrell LJ, Benzel EC, Thompson N, Griffith S, Lieberman IH. Lumbar dorsal root ganglia location: An anatomic and MRI assessment. Int J Spine Surg. 2015;9.

Song XJ, Hu SJ, Greenquist KW, Zhang JM, LaMotte RH. Mechanical and thermal hyperalgesia and ectopic neuronal discharge after chronic compression of dorsal root ganglia. J Neurophysiol. 1999;82(6):3347–58.

Spencer PS, Raine CS, WiśNiewski H. Axon diameter and myelin thickness - unusual relationships in dorsal root ganglia. Anat Rec. 1973;176(2):225–43.

Struijk JJ, Holsheimer J, Boom HBK. Excitation of dorsal root fibers in spinal cord stimulation: A theoretical study. IEEE Trans Biomed Eng. 1993;40(7):632–9.

Struijk JJ, Holsheimer J, van der Heide GG, Boom HBK. Recruitment of dorsal column fibers in spinal cord stimulation: Influence of collateral branching. IEEE Trans Biomed Eng. 1992;39(9):903–12.

Sundt D, Gamper N, Jaffe DB. Spike propagation through the dorsal root ganglia in an unmyelinated sensory neuron: A modeling study. J Neurophysiol. 2015;114(6):3140–53.

Tandrup T. A method for unbiased and efficient estimation of number and mean volume of specified neuron subtypes in rat dorsal root ganglion. J Comp Neurol. 1993;329(2):269–76.

Todd AJ. Neuronal circuitry for pain processing in the dorsal horn. Nat Rev Neurosci. 2010;11:823–36.

Vancamp T, Levy RM, Peña I, Pajuelo A. Relevant anatomy, morphology, and implantation techniques of the dorsal root ganglia at the lumbar levels. Neuromodulation. 2017;20(7):690–702.

Villière V, McLachlan EM. Electrophysiological properties of neurons in intact rat dorsal root ganglia classified by conduction velocity and action potential duration. J Neurophysiol. 1996;76(3):1924–41.

Waxman SG. The molecular pathophysiology of pain: Abnormal expression of sodium channel genes and its contributions to hyperexcitability of primary sensory neurons. Pain. 1999;82(Supplement 6):S133-40.

Waxman SG, Ritchie JM. Organization of ion channels in the myelinated nerve fiber. Science. 1985;228(4707):1502–7.

Welk E, Leah JD, Zimmermann M. Characteristics of A- and C-fibers ending in a sensory nerve neuroma in the rat. J Neurophysiol. 1990;63(4):759–66.

Xiao H-S, Huang Q-H, Zhang F-X, Bao L, Lu Y-J, Guo C, et al. Identification of gene expression profile of dorsal root ganglion in the rat peripheral axotomy model of neuropathic pain. Proc Natl Acad Sci U S A. 2002;99(12):8360–5.

Zhang JM, Donnelly DF, Lamotte RH. Patch clamp recording from the intact dorsal root ganglion. J Neurosci Methods. 1998;79(1):97–103.

Figure legends

Figure 1: Anatomy of the finite element model of a human L5 DRG and stimulating electrode. A) Side view of the DRG with the DRG stimulating electrode oriented above the ganglion (red: active electrode, blue: return electrode, black: inactive electrode). An example primary sensory neuron trajectory is shown in black with the soma below the active electrode. B) Cross sectional view through the middle of the DRG.

Figure 2: Multi-compartment models of primary sensory neurons. A) We modified a previously-published model of a mammalian sensory axon to represent the pseudounipolar morphology of an Aβ-fiber (McIntyre et al. 2002; Amir and Devor 2003; Gaines et al. 2018). An example action potential is shown on the left. The equivalent circuit diagram with active ion conductances included in the nodal, initial segment, and soma compartments is shown on the right. B). We constructed a model of a C-fiber based on morphological parameters and electrophysiological parameters from previous studies (Sheets et al. 2007; Huang et al. 2014; Sundt et al. 2015). An example action potential is shown on the left. The equivalent circuit diagram with active ion conductances included in all membrane compartments is shown on the right.

Figure 3: Coupling the finite element model (FEM) of a human L5 DRG to the multi-compartment models of primary sensory neurons. A) Isopotential lines of the extracellular voltages generated by bipolar DRGS calculated from the FEM. B) Time-dependent transmembrane voltages resulting from stimulating an example Aβ-fiber with a 500 μA anodic DRGS pulse (top trace, gray). The action potential initiates near the soma and then propagates into the central and peripheral axons (bottom three traces, black).

Figure 4: DRGS amplitudes required to elicit one or more action potentials (activation threshold) in primary sensory neurons (PSNs) for anodic- and cathodic-first DRGS. A) Sagittal (top) and transverse (bottom) DRG cross sections used to construct the threshold plots in B. Gray shaded regions indicate the locations of PSN somata. Electrode contacts are color coded such that: red=active electrode, blue=return electrode,

black=inactive contact, white=insulated lead body. B) Activation threshold plots for Aβ- and C-fibers. Black contour lines indicate the cutoff for clinical DRGS amplitude ranges (≤ 1 mA). Note the difference in the colorbar scales between the Aβ- and C-fibers.

Figure 5: Applying DRGS to quiescent and spontaneously-active primary sensory neurons. We applied an anodic DRGS pulse (top trace, gray) with an amplitude of 750 μA, a pulse width of 300 μs, and a pulse frequency of 40 Hz to example quiescent and spontaneously-active Aβ- and C-fibers. The somatic membrane potential traces (bottom traces, black) of example Aβ- and C-fibers before and during DRGS are shown. Gray shaded regions indicate when DRGS is applied.

Figure 6: DRGS amplitudes required to elicit one or more action potentials (activation threshold) in primary sensory neurons (PSNs) after shifting the electrode lead such that the active and return electrodes straddle the ganglion. A) Sagittal (top) and transverse (bottom) DRG cross sections used to construct the threshold plots in B. Gray shaded regions indicate the locations of PSN somata. The electrode lead is color coded such that: red=active electrode, blue=return electrode, black=inactive contact, white=insulated lead body. B) Activation threshold plots for Aβ- and C-fibers. Black contour lines indicate the cutoff for clinical DRGS amplitude ranges (≤ 1 mA). Note the difference in the colorbar scales between the Aβ- and C-fibers.

Table captions

Table 1: Anatomical parameters used to build the finite element model of a human L5 DRG.

Parameter	Value	Reference
DRG length	9.4 mm	(Hasegawa et al. 1996)
DRG width	5.9 mm	(Hasegawa et al. 1996)
Nerve root radius	1.19 mm	(Hogan 1996)
Dural sheath thickness	150 μm	(Reina et al. 2007)
Foramen height	10.1 mm	(Silverstein et al. 2015)
Encapsulation layer	0.3 mm	(Grill and Mortimer 1994)
Electrode contact length	1.25 mm	(Amirdelfan et al. 2018)
Electrode radius	0.5 mm	(Amirdelfan et al. 2018)

Abbreviations: DRG, dorsal root ganglion.

Table 2: Electrical conductivities used in the finite element model.

Parameter	Value	Reference
Gray matter	0.23 S/m	(Geddes and Baker 1967)
White matter (longitudinal)	0.6 S/m	(Geddes and Baker 1967)
White matter (transverse)	0.083 S/m	(Geddes and Baker 1967)

Dural covering	0.6 S/m	(Lempka et al. 2015)
Bone	0.02 S/m	(Gabriel et al. 1996)
General tissue	0.25 S/m	(Geddes and Baker 1967)
Encapsulation	0.17 S/m	(Grill and Mortimer 1994)

Table 3: Cell morphology parameters used to construct the Aβ- and C-fiber multi-compartment models.

Parameter	Aβ-fiber Value	C-Fiber Value	Reference
Fiber diameter (peripheral)	7.3 μm	0.8 μm	(Ha 1970; Lee et al. 1986)
Fiber diameter (central)	5.7 μm	0.4 μm	(Ha 1970; Lee et al. 1986)
Fiber diameter (stem)	7.3 μm	1.4 μm	(Lee et al. 1986; Sundt et al. 2015)
Stem axon length	789 μm	844 μm	(Ito and Takahashi 1960; Amir and Devor 2003; Sundt et al. 2015)
Soma length	80 μm	25 μm	(Ito and Takahashi 1960; Amir and Devor 2003; Sundt et al. 2015)
Soma diameter	80 μm	25 μm	(Ito and Takahashi 1960; Amir and Devor 2003; Sundt et al. 2015)
Node length	1.0 μm	-	(McIntyre et al. 2002)
Heminode diameter	5 μm	-	(Ito and Takahashi 1960; Amir and Devor 2003)
Initial segment length	200 μm	-	(Ito and Takahashi 1960; Amir and Devor 2003)
Initial segment diameter	5 μm	-	(Ito and Takahashi 1960; Amir and Devor 2003)
Paranode length	3.0 μm	-	(McIntyre et al. 2002)
Juxtaparanode length	Variable	-	(McIntyre et al. 2002)
Internode length	Variable	-	(McIntyre et al. 2002; Amir and Devor 2003)

Table 4: Validation metrics for our multi-compartment models against experimental data.

Aβ-Fiber			
Parameter	**Our Value:**	**Literature Ranges**	**Reference**
Soma AP amplitude	107.7 mV	109.72 +/- 11.21 mV	(Huxley and Stämpfli 1951; Amir and Devor 2003)
AP duration (base)	1.225 ms	1.29 +/- 0.59 ms	(Harper and Lawson 1985b)

Rise time	0.775 ms	0.61 +/- 0.13 ms	(Djouhri et al. 1998)
Fall time	0.45 ms	0.89 +/- 0.41 ms	(Djouhri et al. 1998)
Resting potential	-79.1 mV	-80 mV	(Howells et al. 2012)
AHP amplitude	4.2 mV	7.9 +/- 4.2 mV	(Harper and Lawson 1985b)
AHP half-amplitude duration	14.7 ms	10.1 +/- 11.0 ms	(Villière and McLachlan 1996)
Ectopic spiking frequency	28 Hz	10-50 Hz	(Amir et al. 2005)
CV (peripheral axon)	25.00 m/s	14-30 m/s	(Harper and Lawson 1985a)
CV (central axon)	17.02 m/s	14-30 m/s	(Harper and Lawson 1985a)
C-Fiber			
Parameter	**Our Value:**	**Literature Ranges**	**Reference**
Soma AP amplitude	76.5 mV	81.6 +/- 6.9	(Harper and Lawson 1985b)
AP duration (base)	3.5 ms	4.97 +/- 2.16	(Harper and Lawson 1985b)
Rise time	1.675 ms	2.5+/- 0.89	(Djouhri et al. 1998)
Fall time	1.825 ms	4.61 +/- 3.5	(Djouhri et al. 1998)
Resting potential	-55 mV	-48.6 +/- 9.2	(Harper and Lawson 1985b)
AHP amplitude	10.9 mV	8.2 +/- 5.1 mV	(Harper and Lawson 1985b)
AHP half-amplitude duration	5.2 ms	12.87 +/- 8.4 ms	(Harper and Lawson 1985b)
CV (peripheral axon)	0.28 m/s	0.2-0.8 m/s	(Zhang et al. 1998)
CV (central axon)	0.21 m/s	0.2-0.8 m/s	(Zhang et al. 1998)

Abbreviations: AP, action potential; AHP, afterhyperpolarization; CV, conduction velocity.

Figures

Figure 1.

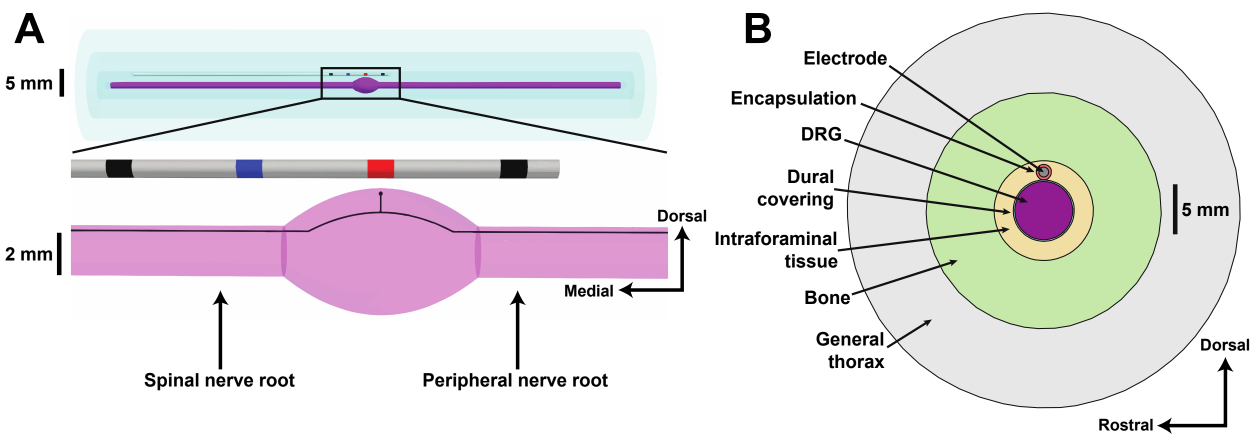

Figure 2.

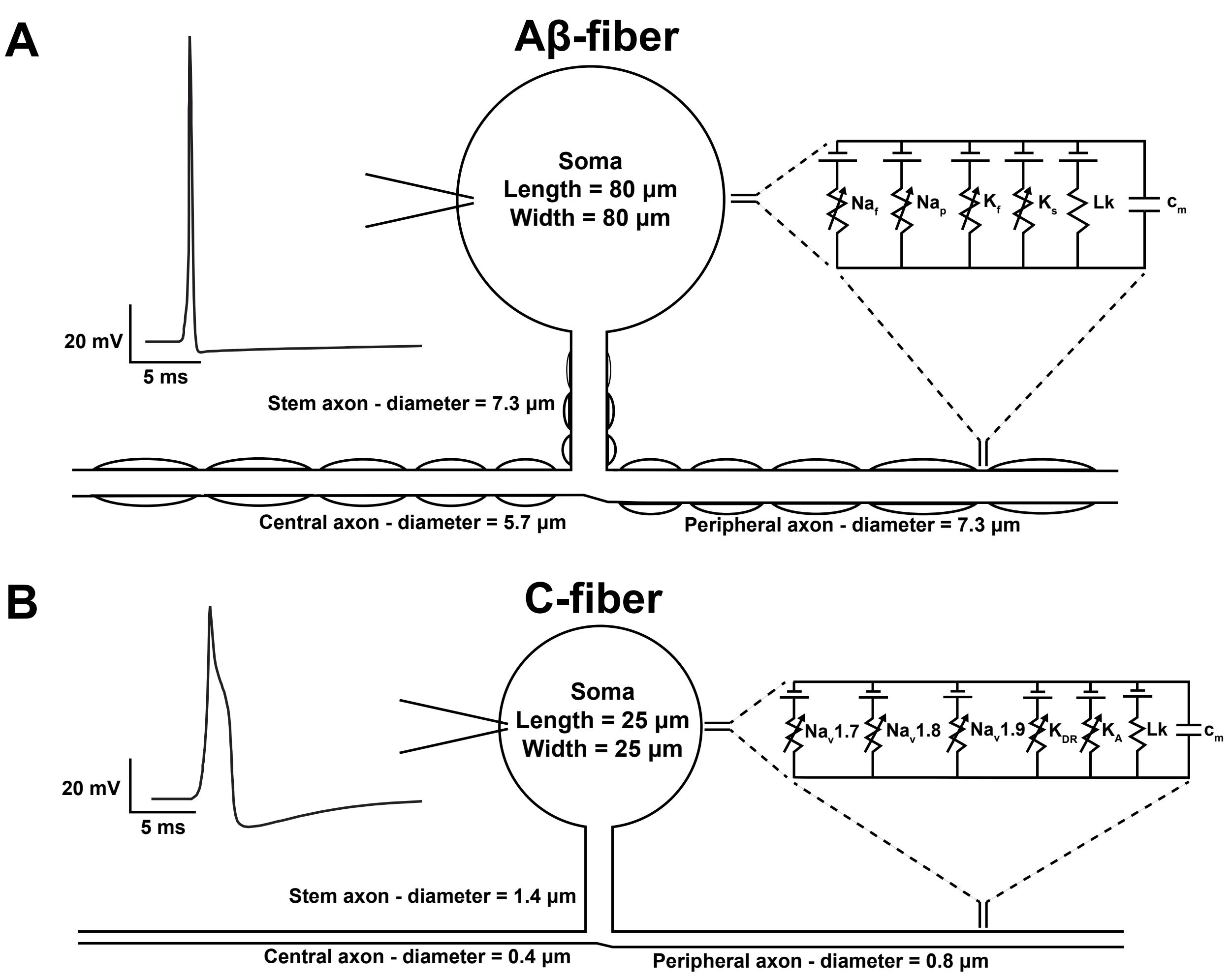

Figure 3.

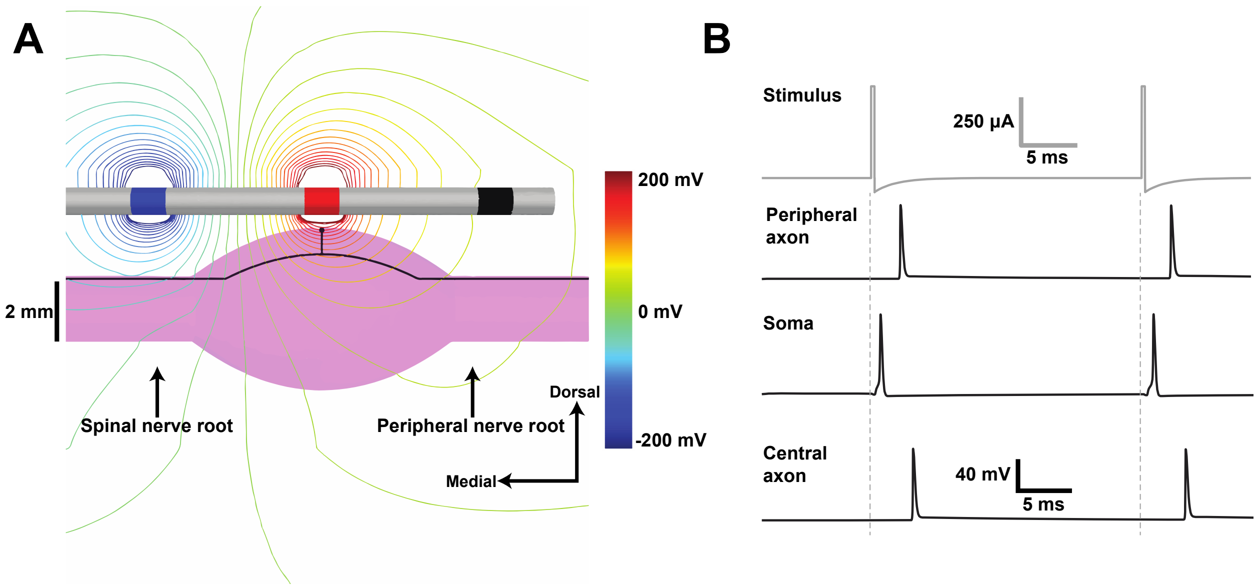

Figure 4.

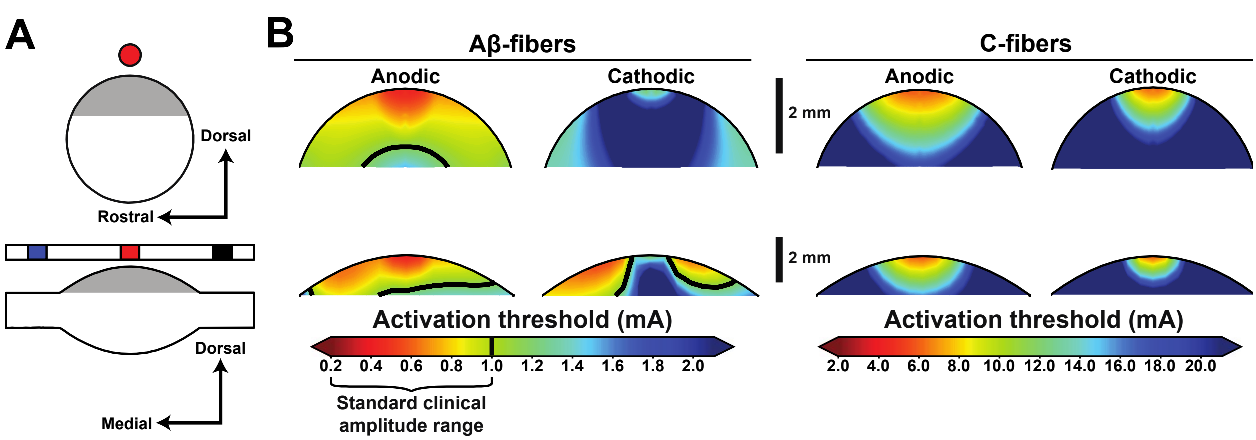

Figure 5.

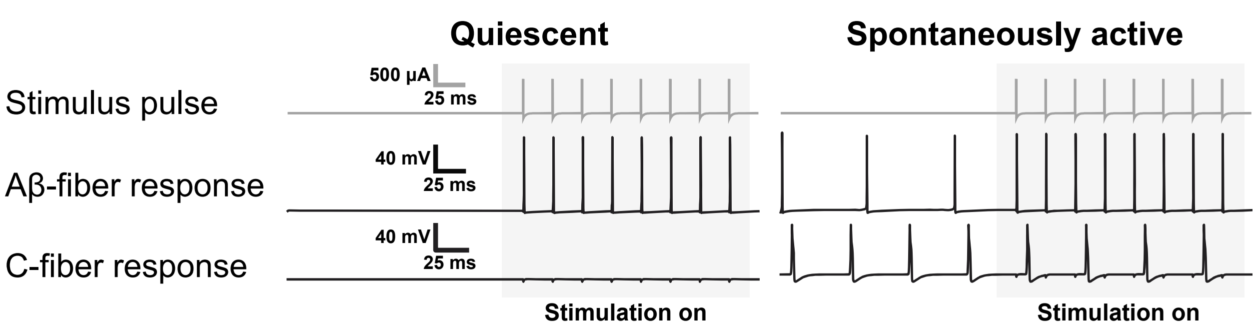

Figure 6.

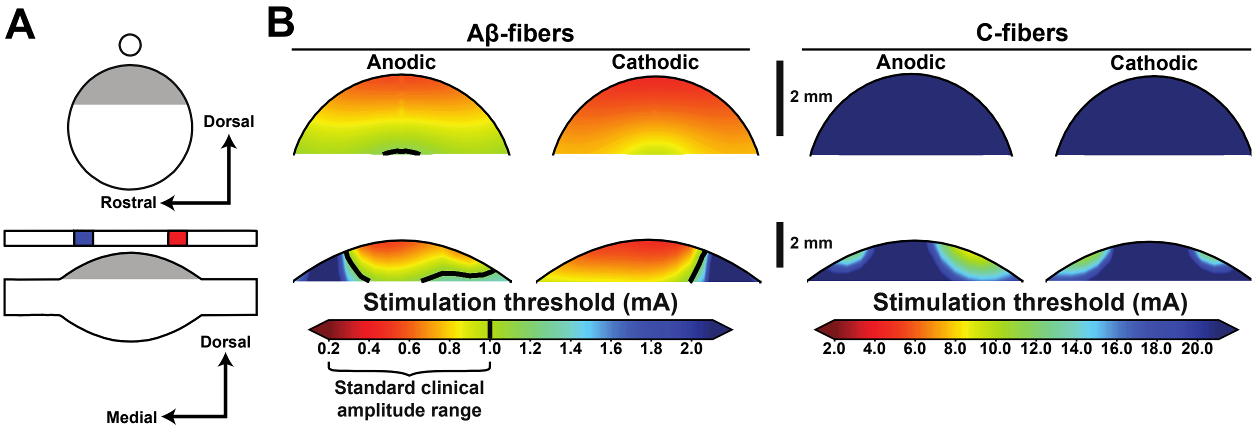

A
Dorsal
Rostral
Dorsal
Medial
B
Aβ-fibers
Anodic
Cathodic
2 mm
C-fibers
Anodic
Cathodic
2 mm
Stimulation threshold (mA)
0.2 0.4 0.6 0.8 1.0 1.2 1.4 1.6 1.8 2.0
Standard clinical amplitude range
Stimulation threshold (mA)
2.0 4.0 6.0 8.0 10.0 12.0 14.0 16.0 18.0 20.0